Ecological Modelling 222 (2011) 653–665

Contents lists available at ScienceDirect

Ecological Modelling

journal homepage: www.elsevier.com/locate/ecolmodel

Modeling the vegetation–atmosphere carbon dioxide and water vapor interactions along a controlled CO_2 gradient

Stefano Manzoni[a,b,*], Gabriel Katul[a,b], Philip A. Fay[c], H. Wayne Polley[c], Amilcare Porporato[a,b]

[a] Nicholas School of the Environment, Box 90328, Duke University, Durham, NC 27708, USA
[b] Department of Civil and Environmental Engineering, Box 90287, Duke University, Durham, NC 27708-0287, USA
[c] USDA-ARS Grassland Soil and Water Research Laboratory, 808 E Blackland Rd, Temple, TX 76502, USA

ARTICLE INFO

Article history:
Received 11 May 2010
Received in revised form 15 October 2010
Accepted 20 October 2010
Available online 17 November 2010

Keywords:
Canopy turbulence
Enclosed environments
Elevated CO_2
Heat exchange
Optimal stomatal conductance
Photosynthesis

ABSTRACT

Ecosystem functioning is intimately linked to its physical environment by complex two-way interactions. These two-way interactions arise because vegetation both responds to the external environment and actively regulates its micro-environment. By altering stomatal aperture, and therefore the transpiration rate, plants modify soil moisture and atmospheric humidity and these same physical variables, in return, modify stomatal conductance. Relationships between biotic and abiotic components are particularly strong in closed, managed environments such as greenhouses and growth chambers, which are used extensively to investigate ecosystem responses to climatic drivers. Model-assisted designs that account for the physiological dynamics governing two-way interactions between biotic and abiotic components are absent from many ecological studies. Here, a general model of the vegetation–atmosphere system in closed environments is proposed. The model accounts for the linked carbon–water physiology, the turbulent transport processes, and the energy and radiative transfer within the vegetation. Leaf gas exchange is modeled using a carbon gain optimization approach that is coupled to leaf energy balance. The turbulent transport within the canopy is modeled in two-dimensions using first-order closure principles. The model is applied to the Lysimeter CO_2 Gradient (LYCOG) facility, wherein a continuous gradient of atmospheric CO_2 is maintained on grassland assemblages using an elongated chamber where the micro-climate is regulated by variation in air flow rates. The model is employed to investigate how species composition, climatic conditions, and the imposed air flow rate affect the CO_2 concentration gradient within the LYCOG and the canopy micro-climate. The sensitivity of the model to key physiological and climatic parameters allows it to be used not only to manage current experiments, but also to formulate novel ecological hypotheses (e.g., by modeling climatic regimes not currently employed in LYCOG) and suggest alternative experimental designs and operational strategies for such facilities.

© 2010 Elsevier B.V. All rights reserved.

1. Introduction

Variability in mass and energy exchange rates between the vegetation and the atmosphere is primarily controlled by fluctuations in the environment (dePury and Farquhar, 1997; Friend, 1995; Landsberg and Waring, 1997; Leuning, 1995; Running and Gower, 1991; Williams et al., 1996), including variability in environmental conditions in the atmospheric layers immediately above the canopy (e.g., radiation, see Stoy et al., 2009). There is now growing interest in the other side of these interactions, which deal with how vegetation regulates these environmental variables (Daly et al., 2004; Siqueira et al., 2009). One way to proceed in exploring these complex two-way interactions is to experimentally amplify them, for instance by using closed environments such as greenhouses or growth chambers, where the boundary layer depth is restricted and the lateral boundaries are controlled. Considering the general interest in quantifying crop growth in greenhouses and the increasing use of growth chambers to investigate ecosystem responses to altered climatic conditions (Fay et al., 2009; Johnson et al., 2000), it is imperative to formulate mathematical models of vegetation–atmosphere interactions in such closed systems.

Models describing the energy and water vapor balances of greenhouse systems have been used to characterize micro-environmental conditions and to improve greenhouse design (Boulard and Baille, 1993; Boulard et al., 2002; Kindelan, 1980; Majdoubi et al., 2009; Roy et al., 2002; Singh et al., 2006; Soribe and Curry, 1973; Teitel et al., 2010; Willits, 2003; Yang et al., 1990). These models generally neglect or over-simplify photosynthesis and transpiration, thus missing the alterations induced by the vegetation to the canopy micro-climate. These two-way interactions

* Corresponding author at: Nicholas School of the Environment, Box 90328, Duke University, Durham, North Carolina 27708, USA. Tel.: +1 919 6605467; fax: +1 919 6605219.
E-mail address: stefano.manzoni@duke.edu (S. Manzoni).

0304-3800/$ – see front matter © 2010 Elsevier B.V. All rights reserved.
doi:10.1016/j.ecolmodel.2010.10.016

are critical to plant feedbacks to the atmosphere, and thus these models are not directly applicable to growth chambers designed to assess the effects of climatic changes on vegetation. On the other hand, canopy models are now available that incorporate physiological, radiative, and turbulent transport descriptions of vegetation–atmosphere interactions in open systems (Baldocchi and Meyers, 1998; Daly et al., 2004; Juang et al., 2008; Lai et al., 2002; Siqueira et al., 2006; Tuzet et al., 2003). These models may be adapted to resolve both vegetation and atmosphere contributions to coupled energy and mass fluxes in closed systems, allowing integration at seasonal to annual time scales on which ecological processes operate.

Here, a general soil–vegetation–atmosphere model applicable under both natural conditions and in closed environments is proposed. The major advances in this model formulation are: (i) generalization of an existing stomatal optimization scheme to account for the effects of leaf boundary layer and energy balance, and the implementation of this scheme in a multi-layer canopy model; (ii) inclusion of atmospheric scalar advective components to describe vegetation–atmosphere interactions in closed systems with ventilation. The model is then used to quantify water and carbon dioxide fluxes in grassland vegetation grown along a continuous gradient in atmospheric CO_2 concentration. The gradient was created by introducing CO_2 enriched air into a linear sequence of chamber compartments, where photosynthesis progressively depleted the air of CO_2 during advection through the chambers (Fay et al., 2009; Johnson et al., 2000). The shape of the CO_2 concentration gradient is controlled by a combination of biological components, primarily species composition and photosynthetic capacity, and physical components, chiefly the transit time of air through the chambers and the degree of atmospheric mixing. The proposed model is employed to assess the sensitivity of the system to both components, thus providing a mechanistic link between management options (e.g., controlling air flow rate within the chamber system) for regulating the desired CO_2 gradient. This model allows for a complete characterization of vegetation–atmosphere coupling under CO_2 concentrations spanning pre-industrial to mid-21st century conditions.

2. Methods

2.1. Theory

The model couples soil–vegetation–atmosphere dynamics (Fig. 1) at a temporal scale commensurate with averaging times of meteorological variables (~30 min). These time scales are sufficiently long to average over turbulent time scales (~10 s) but short enough to resolve diurnal variations in the meteorological drivers. The soil compartment is assumed to be lumped in space, whereas the vegetation and atmospheric compartments are resolved in the vertical dimension (~0.1 m). In the following, the model components are briefly described. Symbols used in the atmosphere, canopy, leaf-level, and soil-to-leaf conductance calculations are listed and explained in appendix Tables A1–A4, respectively.

2.1.1. Momentum and scalar mass balances

Mean air velocity U and scalar transport within and above the canopy are modeled using a modified version of the CANVEG approach (Baldocchi and Meyers, 1998; Lai et al., 2002; Siqueira et al., 2006). For the discussion here, we align the coordinate system with x being the longitudinal and z the vertical directions, respectively, with the longitudinal being the mean wind direction (Fig. 1). In the absence of subsidence, the mean velocity U is computed by solving the momentum balance equation in a stationary

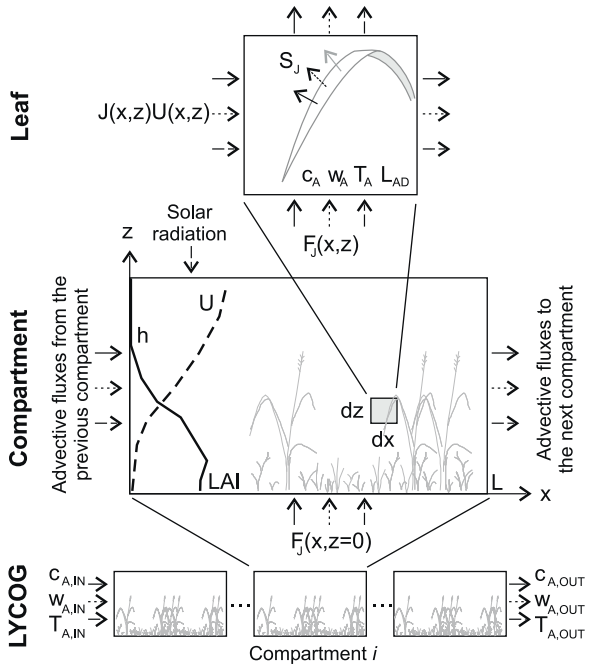

Fig. 1. Schematic representation of the coupled vegetation–atmosphere model. Leaf-level gas and heat exchange fluxes (Sections 2.1.4 and 2.1.5) are up-scaled to the canopy level by coupling sources for scalar J at a given position (S_J) to atmospheric turbulent transport equations (solid arrows: CO_2 fluxes; dotted arrows: water fluxes; dashed arrows: heat fluxes; see Section 2.1.1). Canopy-scale calculations are further up-scaled to the whole chamber level by accounting for advective transport. To describe the LYCOG facility, several compartments in series and linked by plenums containing air coolers are considered (Section 2.3).

planar homogeneous system at high Reynolds number,

$$\frac{\partial F_M}{\partial z} = C_d L_{AD} U^2, \tag{1}$$

where F_M is the vertical flux of momentum, L_{AD} is the (measured) leaf area density and the drag coefficient $C_d = 0.3$, a typical value for dense canopies (Boulard et al., 2002; Katul et al., 2004; Poggi et al., 2004). Even for stationary conditions and in the absence of subsidence, the complete mean momentum budget would require the retention of the mean pressure gradient, the longitudinal advective term, and the longitudinal gradient of the horizontal velocity variance produced by turbulence. However, we assume here that the flow field attains its one-dimensional status far more rapidly than the scalar field so that for our purposes, we can neglect this rapid longitudinal adjustment of the flow as it enters the chamber compartments. The fact that the mean momentum budget adjusts over much shorter distances when compared to the mean scalar budgets as the flow encounters a step change in boundary conditions has been studied extensively (Hsieh and Katul, 2009; Rao et al., 1974). For a stationary and a high Peclet number flow, the atmospheric mean mass balances for a generic scalar J such as water vapor concentration, CO_2 concentration, or air temperature (see Table A1 for details) can be written as

$$U\frac{\partial J}{\partial x} + \frac{\partial F_J}{\partial z} = S_J, \tag{2}$$

where advection of the scalar J by the mean longitudinal flow, and the variation of the mean turbulent vertical fluxes F_J, are balanced by the emission (or uptake) rate, S_J. Here, the horizontal gradients of the longitudinal turbulent fluxes are neglected though they can be readily accommodated if they are significant. Sources and sinks of CO_2, water vapor, and sensible heat within the canopy are calculated by multiplying the local leaf area density by the leaf-level

assimilation rate, transpiration rate, and sensible heat sources or sinks (described in Sections 2.1.4 and 2.1.5; see Fig. 1).

The mean vertical momentum (subscript M) and scalar fluxes (subscript J) are computed through a first-order turbulent closure scheme (assuming that the turbulent Schmidt number for scalar J is unity),

$$F_M = -k_t \frac{\partial U}{\partial z}, F_J = -k_t \frac{\partial J}{\partial z}. \quad (3)$$

The turbulent diffusivity k_t is described as

$$k_t = \ell^2 \left| \frac{\partial U}{\partial z} \right|, \quad (4)$$

where the mixing length ℓ is given by (Katul et al., 2004; Poggi et al., 2009)

$$\ell = \kappa h \left(1 - \frac{d}{h}\right), \quad (5)$$

where the d is the centroid height of the drag force. This simplified modeling approach is consistent with the overall level of detail of the model and is supported by previous successful use in both open and closed environments (Katul et al., 2004; Poggi et al., 2009, 2004; Yang et al., 1990). In general, first-order closure principles are applicable when the production term is balanced by the dissipation term in the scalar flux budget with minimal contributions from the gradients in the turbulent flux transport terms. As explained in Appendix B, this condition is generally satisfied in the LYCOG canopy. For application of the model to closed chambers with smooth cover, the typical linear increase in mixing length for $z > d$ (Katul et al., 2004) was not considered (Eq. (5)) due to the presence of the physical boundary imposed by the cover just above the canopy top.

2.1.2. Boundary conditions

Air velocity at the top of the domain was set to conserve air mass for a given flow rate, while $U(0) = 0.01\ \mathrm{m\ s^{-1}}$ was set at the bottom to ensure that the air flow remains fully turbulent and the exchange rates between the ground and the air near the ground can be modeled via k_t without any molecular diffusion contributions. Alternative (though no less arbitrary) formulations may approximate the ground as a pure boundary layer and employ the log-law formulation assuming a ground momentum roughness length. Zero-flux top boundary conditions were imposed for water vapor and CO_2, because the physical barrier imposed by the chamber cover blocks such exchanges. Skin temperature at the chamber cover was assumed equal to the outside temperature (i.e., we assume that the chamber cover is sufficiently thin and highly transmissive), and well-coupled with outside and inside air due to the presence of sustained wind. We also imposed a flux boundary condition at the soil surface for all three scalars. We assumed that soil evaporation is negligible with respect to transpiration (e.g., Boulard and Baille, 1993; Teitel et al., 2010), while we used an empirical temperature-dependent soil respiration function (based on observations) as boundary condition for CO_2.

We set the sensible heat flux from the ground H_G as a boundary condition for the energy conservation equation. The ground surface temperature needed to define H_G was computed from a simplified steady-state model of the ground surface energy balance (Kindelan, 1980; Singh et al., 2006) that considers absorbed shortwave radiation (Campbell and Norman, 1998 and Section 2.1.3 below), sensible heat flux to the atmosphere, and thermal losses to the deeper soil layers. For simplicity, we also assume that the ground surface (predominantly consisting of leaf litter) have the same spectral properties of the leaves in the canopy and the boundary layer conductance of the ground surface is approximated as a leaf boundary layer conductance with characteristic length scale of 0.0075 m. The mean soil thermal conductivity is modeled after Campbell and Norman (1998), and the soil temperature at a depth of $Z_r/2$ was set to 25 °C.

2.1.3. Canopy radiation balance

Photosynthesis and leaf energy balance are controlled by incoming shortwave radiation at each level in the canopy, which is described by a simplified radiation attenuation model (see details in Goudriaan and van Laar, 1994; Leuning et al., 1995; Spitters, 1986). We accounted for near infrared and visible bands separately, while we neglected the longwave radiation balance in this closed system where emissivity and temperature differences between radiating surfaces are relatively small. Total incoming solar radiation was partitioned between visible (a fraction $f_V = 0.45$) and near infrared components (a fraction $f_{NIR} = 0.55$). Absorbed shortwave radiation in the canopy (per unit leaf area) was described by different exponential attenuation profiles, depending on the waveband (indicated by subscript i: near infrared, $i = NIR$; visible, $i = V$), following Goudriaan and van Laar (1994),

$$Q_i = Q_i^{\downarrow} (1 - \rho_i) \sqrt{1 - \sigma_i} k \exp\left(-\sqrt{1 - \sigma_i} k \xi\right), \quad (6)$$

where $Q_i^{\downarrow}$ is the incoming radiation at the top of the canopy, ξ the cumulative leaf area index profile, σ_i the scattering coefficients, k the extinction coefficient, and ρ_i the canopy reflection coefficients (see details in Table A2),

$$\rho_i = \frac{2k}{k + k_D} \frac{1 - \sqrt{1 - \sigma_i}}{1 + \sqrt{1 - \sigma_i}}. \quad (7)$$

The total net absorbed radiation at each level in the canopy was found as the sum of all spectral components, $Q_n = Q_V + Q_{NIR}$.

2.1.4. Leaf gas exchange

Transpiration and net assimilation fluxes across the stomata were described by Fickian diffusion,

$$E = g_{LA,W} (w_{sat}(T_L) - w_A), \quad (8)$$

$$A = g_{LA,C} (c_A - c_I), \quad (9)$$

where $w_{sat}(T_L)$ and w_A are water vapor concentrations at saturation (at leaf temperature) and in the bulk atmosphere, c_A and c_I are the atmospheric and internal CO_2 concentrations, and $g_{LA,W}$ and $g_{LA,C}$ are the leaf–atmosphere conductances, computed from the series of stomatal and boundary layer conductances to water vapor and CO_2, respectively, i.e., $g_{LA,j} = g_{S,j} g_{B,j} / (g_{S,j} + g_{B,j})$. The leaf boundary layer conductance was calculated as a function of wind speed and leaf characteristic width d_L (Campbell and Norman, 1998). The coefficients to convert conductances for water vapor to conductances for CO_2 or heat are reported in Table A3 (see details in Bonan, 2008; Campbell and Norman, 1998).

The CO_2 demand set by the leaf photosynthetic capacity can be expressed as a multiplicative function of light limitation and CO_2 limitation terms (Berninger and Hari, 1993; Hari et al., 1986). The CO_2 limitation term is here obtained by linearizing the Rubisco-limited photosynthesis kinetics from the Farquhar model (Farquhar et al., 1980). The linearization was carried out assuming that in the denominator internal CO_2 concentration is approximated as $c_I \approx R_C c_A$ where R_C is the long-term average c_I/c_A (Katul et al., 2009). As a result, A is expressed as,

$$A = \frac{a_1 Q_P}{Q_P + \gamma} \frac{\eta c_I - \Gamma}{\eta R_C c_A + a_2} - R_d, \quad (10)$$

where Γ is the CO_2 compensation point, $R_d = 0.01 a_1$ is the mitochondrial respiration, a_1, a_2, and γ are kinetic constants that depend on leaf water potential and temperature, η is the efficiency of the CO_2 pump in C4 species (set to unity in C3 species), and Q_P is the

absorbed photosynthetic active radiation (Eq. (6)). The linearization of Eq. (10) is justified by the fact that changes in c_I are mainly due to changes in c_A, allowing the approximation $c_I \approx R_C c_A$. Note that the internal CO_2 concentration can still change in response to altered balance of CO_2 supply and demand, thus capturing the biochemical couplings between stomatal conductance and photosynthesis. The rate coefficient a_1 represents the carboxylation rate and $a_2 = K_C(1 + [O_2]/K_O)$ accounts for the balance of carboxylation and oxygenation reactions. The impairment of photosynthetic capacity under water stress (represented by increasingly negative leaf water potentials Ψ_L) is accounted for by means of an empirical curve that decreases the maximum rate under well-watered (WW) conditions (Vico and Porporato, 2008),

$$a_1 = a_{1,WW} \exp\left[-\left(\alpha_1 \left|\psi_L\right|\right)^{\alpha_2}\right]. \tag{11}$$

Specific expressions for the temperature effects on $a_{1,WW}$, a_2, and Γ are reported by Leuning (1995). Eqs. (8)–(10) allow computing three of the four unknowns (i.e., CO_2 and water vapor fluxes, internal CO_2 concentration, and stomatal conductance). To mathematically close the problem, a further equation must be introduced to define stomatal conductance, $g_{S,C}$. Because of the complex feedbacks between energy and water fluxes and $g_{S,C}$, it is more convenient to first define leaf temperature and water potential, and later present the expression for $g_{S,C}$ (Section 2.1.7).

2.1.5. Leaf energy balance

The leaf energy balance can be written as (Campbell and Norman, 1998)

$$Q_n = LE + H, \tag{12}$$

where the absorbed radiation (Q_n) is balanced by latent (LE) and sensible (H) heat fluxes (i.e., leaf temperature is assumed in equilibrium at the half-hourly time scale). The latent heat flux is computed from Eq. (8), while the sensible heat exchange between the leaf and the atmosphere is given by

$$H = C_p g_{B,H} (T_L - T_A), \tag{13}$$

where $g_{B,H}$ is the leaf boundary layer conductance for sensible heat. A suitable approximation for leaf temperature is obtained by neglecting the longwave contribution and linearizing Eq. (12), (Campbell and Norman, 1998),

$$T_L = T_A + \frac{Q_n - \Lambda g_{LA,W} D}{C_p g_{B,H} + \Lambda g_{LA,W} s}. \tag{14}$$

In this way, all quantities on the right hand side of Eq. (14) depend on air temperature and stomatal and boundary layer conductances only. As it will be clear in the following, this formulation is useful for an efficient implementation of the stomatal model in the fully coupled vegetation–atmosphere model (Section 2.2).

2.1.6. Soil–vegetation–atmosphere continuum

Because water storage within the vegetation-system is ignored (as vegetation in such controlled environments is relatively short-statured), the transpiration flux (Eq. (8)) must be conserved throughout the soil–vegetation–atmosphere system,

$$E = g_{SL}\left(\psi_S - \psi_L\right), \tag{15}$$

where Ψ_L and Ψ_S are leaf and soil water potentials, respectively, and g_{SL} is the soil-to-leaf conductance to water. Eq. (15) can be inverted to compute the leaf water potential,

$$\psi_L = \psi_S - \frac{E}{g_{SL}}. \tag{16}$$

Note that Ψ_L depends on E, which in turn is a function of stomatal conductance and leaf–atmosphere water vapor gradient (Eq. (8)), so that $\Psi_L = \Psi_L(g_{S,C})$.

The soil-to-leaf conductance was computed as the series of soil-to-root conductance g_{SR} (dominant at low soil moisture), and root-to-leaf conductance g_{RL} (dominant at high soil moisture and assumed constant for simplicity), as $g_{SL} = g_{SR} g_{RL}/(g_{SR} + g_{RL})$. The soil-to-root conductance is modeled after Daly et al. (2004),

$$g_{SR} = \varphi K_H\left(\psi_S\right)\sqrt{\frac{R_{AI}}{2 d_R Z_R w_S^v}}, \tag{17}$$

where K_H is the soil hydraulic conductivity, R_{AI} the root area index, d_R the root radius, Z_R the rooting depth, w_S^v a correction factor to account for root elongation under low soil moisture, and $\varphi = 10^9/(18 \times 9.81)$ a coefficient to convert the conductance units to mol m^{-2} s^{-1} MPa^{-1}.

2.1.7. Optimal stomatal conductance model

Stomatal conductance is modeled using an optimization approach based on the economics of gas exchange. An implicit expression to be solved for $g_{S,C}$ is derived by maximizing the leaf assimilation rate A, subject to the constraint that leaf $E > 0$ (Berninger and Hari, 1993; Cowan and Farquhar, 1977; Katul et al., 2009). To achieve this, we maximize the leaf C gain function, $f = A - \lambda E$, where λ is the marginal water use efficiency (the Lagrange multiplier for the problem), by imposing $\partial f/\partial g_{S,C} = 0$, and thus obtain an expression for $g_{S,C}$. When the boundary layer resistance is assumed negligible and leaf water potential and temperature can be considered externally imposed parameters (as in the case of well-mixed leaf gas exchange cuvettes), the derivation of an explicit, analytical expression for $g_{S,C}$ is straightforward (Berninger and Hari, 1993; Hari et al., 1986; Katul et al., 2010; Manzoni et al., 2010). When the effects of stomatal conductance on leaf water status and temperature are considered (see Sections 2.1.5 and 2.1.6), the optimality condition becomes rather unwieldy and does not admit an analytical solution for $g_{S,C}$ (e.g., Buckley et al., 2002). Here the optimality condition is derived for the general case.

Leaf temperature is controlled by stomatal conductance (Eq. (14)), but it also controls the water vapor concentration in the stomatal cavity and thus the driving force of transpiration (Eq. (8)). As a consequence, we can express the transpiration flux as $E = E[g_C, T_L(g_C)]$ (Eq. (8)). The assimilation flux can be also written as a function of stomatal conductance (by combining Eqs. (9) and (10) and eliminating c_I), and leaf temperature and water potential (Eqs. (10) and (11)). Leaf temperature and water potential are in turn controlled by stomatal conductance (Eqs. (14) and (16), respectively), so that $A = A\left[g_C, \psi_L(g_C), T_L(g_C)\right]$. As a result, the optimality condition can be written as

$$\frac{\partial f\left[g_{S,C}, \psi_L, T_L\right]}{\partial g_{S,C}} = \left.\frac{\partial A}{\partial g_{S,C}}\right|_{\psi_L, T_L} + \left.\frac{\partial A}{\partial T_L}\right|_{g_{S,C}, \psi_L}\frac{\partial T_L}{\partial g_{S,C}} + \left.\frac{\partial A}{\partial \psi_L}\right|_{g_{S,C}, T_L}\frac{\partial \psi_L}{\partial g_{S,C}} - \lambda\left(\left.\frac{\partial E}{\partial g_{S,C}}\right|_{\psi_L, T_L} + \left.\frac{\partial E}{\partial T_L}\right|_{g_{S,C}, \psi_L}\frac{\partial T_L}{\partial g_{S,C}}\right) = 0, \tag{18}$$

which can only be solved numerically for the unknown $g_{S,C}$.

The marginal water use efficiency λ varies with large changes in c_A and plant water status (Katul et al., 2010; Manzoni et al., 2010). In the drought resistant grassland species considered here, the sensitivity of λ to water availability has been shown to be not significant, while the CO_2 effect is nearly linear (Manzoni et al., 2010). This yields the relationship,

$$\lambda(c_A) = \lambda^* \frac{c_A}{c_A^*}, \tag{19}$$

where λ^*, the marginal water use efficiency at the reference $c_A^* = 400\,\mu$mol mol^{-1}, is the only parameter to be calibrated against gas exchange measurements (Section 2.3). As discussed by Katul

et al. (2010), Eq. (19) also recovers the well-known proportionality between $g_{S,C}$ and A/c_a assumed in leaf-level formulations such as the Leuning (1995) approach.

2.2. Numerical implementation

The canopy model has been implemented in Matlab (The MathWorks, Inc.) using two nested routines. One performs the leaf-level calculations, which are used to compute the scalar sources at each canopy level necessary for the second routine to solve the atmospheric scalar transport equations. Leaf-level calculations are complicated by the solution of the optimality equation for stomatal conductance. The iterative scheme designed to numerically solve the problem is outlined below. Given an initial guess for stomatal conductance $g^*_{S,C}$, leaf temperature (Eq. (14)), water potential (Eq. (16)), and internal CO_2 concentration (expressed as a function of $g_{S,C}$, T_L, and Ψ_L by combining Eqs. (9) and (10)) are computed. Second, the partial derivatives of T_L, Ψ_L, and c_I with respect to $g_{S,C}$ are calculated assuming $g_{S,C} = g^*_{S,C}$. Third, the optimality condition (Eq. (18)) is written as

$$\frac{\partial f}{\partial g_{S,C}} = \left.\frac{\partial A}{\partial g_{S,C}}\right|_{\psi_L,T_L} + \left.\frac{\partial A}{\partial c_I}\right|_{\psi_L,T_L}\frac{\partial c_I}{\partial g_{S,C}} - \lambda\left(\left.\frac{\partial E}{\partial g_{S,C}}\right|_{\psi_L,T_L} + \left.\frac{\partial E}{\partial T_L}\right|_{g_{S,C},\psi_L}\frac{\partial T_L}{\partial g_{S,C}}\right) = 0. \tag{20}$$

Using Eqs. (8) and (9), Eq. (20) can be inverted to provide a new estimate for $g_{S,C}$,

$$g_{S,C} = \frac{(c_A - c_I)\left(\chi_{S,W:C} + \chi_{B,W:C}\frac{g_{B,C}}{g^*_{S,C}}\right) - \chi_{S,W:C}\chi_{B,W:C}\lambda\left(1 + \frac{g_{B,C}}{g^*_{S,C}}\right)[w_{sat}(T_L) - w_A]}{\left(\chi_{S,W:C} + \chi_{B,W:C}\frac{g_{B,C}}{g^*_{S,C}}\right)\frac{\partial c_I}{\partial g_{S,C}} + \chi_{B,W:C}\lambda s(T_L)\left(1 + \frac{g_{B,C}}{g^*_{S,C}}\right)\frac{\partial T_L}{\partial g_{S,C}}}, \tag{21}$$

where the partial derivative of c_I contains the effects of leaf temperature and water potential on the photosynthesis parameters (the other coefficients are defined in Table A3). Eq. (21) is solved iteratively until convergence to a specified accuracy is achieved. A maximum value for $g_{S,C}$ is also set to avoid unrealistically high conductances at low D. The numerical solution has also been compared against the theoretical results reported by Manzoni et al. (2010) in the case of negligible boundary layer and soil-to-leaf resistances with excellent agreement between these results and the numerical solution.

2.3. Application to the Lysimeter CO_2 gradient (LYCOG)

As a case study, the species physiological differences that affect optimal leaf gas exchange parameters are investigated in terms of longitudinal scalar gradients that develop in the closed environment of the Lysimeter CO_2 Gradient (LYCOG) facility (located in Temple, TX). The LYCOG facility is used to expose grassland vegetation consisting of mixtures of C4 grasses and C3 forbs to a continuous gradient of atmospheric CO_2 concentration (250–500 μmol mol^{-1}). The gradient of CO_2 is maintained by blowing enriched air into elongated chambers (composed of 20, 5-m-long compartments, as schematically depicted in Fig. 1) and allowing the vegetation to deplete CO_2 from the air stream through photosynthesis. Both temperature and water vapor concentrations are regulated by means of cooling coils located at the compartment joints to match the outside conditions. The chambers are enclosed by a thin (0.15 mm), clear polyethylene cover with ~90% transmissivity that minimally alters the light spectrum (Johnson et al., 2000). Grassland vegetation is allowed to grow in intact soil monoliths of three soil types (varying in texture and fertility), each replicated along the CO_2 gradient. Irrigation schedule and amounts also match typical rainfall patterns of the area. Further details about the experiment are reported elsewhere (Fay et al., 2009; Polley et al., 2008).

For the present sensitivity analyses, we modeled the LYCOG system as a continuous sequence of 5-m-long compartments joined by plenums that perfectly mix the air stream and reduce temperature and humidity to specified values (equal to the external conditions). For simplicity, we neglected air losses from the chambers and changes in pressure that result from the use of fans located adjacent to some of the plenums. Also, we assumed a single-species canopy of *Solidago canadensis* (the dominant C3 forb), or *Sorghastrum nutans* (the dominant C4 grass), growing on a single soil type. This simplified representation of the experimental facility and canopy structure allows us to focus on the interactions between the leaf-level biochemical features of these two species and their chamber environment. Hence, minimal model calibration was carried at the leaf level only, while the atmospheric flow sub-model was validated against observed velocity profiles (described below). Typical mid-summer external environmental conditions are assumed for all simulations.

Vertical profiles of mean longitudinal velocity were measured during July 2009 using T-AVM430 hot wire anemometers (Topac Instrumentation, Cohasset, MA, USA). For different fan speeds and at different locations in the chamber, five or six velocity readings (30 s averages) were recorded after equilibration of the anemometer at each of 8–10 locations in the vertical at each point considered in the chamber. LAI profiles for the sampling day were obtained by linearly interpolating in time LAI profiles measured during June and September 2009. We also assumed that the LAI of the 0–10 cm canopy layer (which can not be measured due to space constraints) was approximately equal to the 10–20 cm value.

The values of the physiological parameters used are reported in Table 1. We calibrated the leaf-level photosynthesis model (Eq. (10)) and the marginal water use efficiency function (Eq. (19)) using CO_2 and light response curves from non-stressed leaves, as well as individual steady-state gas exchange measurements for *S. canadensis* and *S. nutans*. All gas exchange measurements were performed during the 2006, 2007, and 2008 growing seasons using an open path photosynthesis system (LI-6400, LiCor Biosciences, Lincoln, NE, USA). Parameters $a_{1,WW}$ and a_2 (at a reference temperature of 25 °C) were estimated by fitting Eq. (10) to the light-saturated CO_2 response curves (Fig. 2a). The half saturation constant γ was similarly obtained by nonlinear fitting of the light response curves (Fig. 2b). Parameters for Eq. (19) were obtained by fitting the marginal water use efficiency estimates for both species along CO_2 and water availability gradients (Manzoni et al., 2010). Observed CO_2 response curves and concomitant leaf water potentials were used to estimate the leaf photosynthetic capacity a_1 and its sensitivity to water stress. We did not find significant changes in a_1 over the available range of leaf water potentials, e.g., between about −1 and −2.5 MPa. Hence, we used the values for α_1 and α_2 (Eq. (11)) typical for stress-resistant species as reported by Vico and Porporato (2008).

The soil-to-leaf conductance model was parameterized for a sandy loam soil using hydraulic conductivity parameters reported by Laio et al. (2001) and assuming for both species a root area of 80 m^2/m^2 (a typical value for grasslands, see Jackson et al. (1997)) mostly contained within a rooting depth Z_R = 0.3 m (Fay et al., 2009). The root-to-leaf conductance was adjusted to have leaf water potentials around the measured value of −1 MPa under well-watered conditions (Table 1). Soil respiration (the lower-boundary condition for the CO_2 mass balance equation) was obtained from CO_2 efflux measured with a LI-6400 connected to soil respiration chambers (Fay et al., 2009). The Kirschbaum (1995) temperature sensitivity model was used to account for temperature effects on respiration. To fit the model, we maintained the original optimum

Table 1
Values of physiological parameters used for the two grassland species considered (symbols are explained in Table A3). Temperature corrections for the kinetic constants are reported by Leuning (1995).

Parameter	*S. canadensis*	*S. nutans*	Units	Source
$a_{1,WW}$ (25 °C)	20.3	15.9	μmol m^{-2} s^{-1}	Calibrated (Fig. 2)
d_L	0.008	0.004	m	Personal observation
d_R	0.001	0.001	m	Thornley and Johnson (1990)
g_{RL}	0.005	0.005	mol m^{-2} s^{-1} MPa^{-1}	Calibrated from Ψ_L under well-watered conditions
$g_{S,C,max}$	0.4	0.2	mol m^{-2} s^{-1}	Available gas exchange measurements
K_C (25 °C)	119	555	μmol mol^{-1}	Calibrated (Fig. 2)
K_o	677	450	mol mol^{-1}	Leuning (1995), von Caemmerer (2000)
R_{AI}	80	80	m^2 m^{-2}	Jackson et al. (1997)
R_d	$0.01a_1$	$0.01a_1$	μmol m^{-2} s^{-1}	Buckley (2008)
R_C	0.7	0.4	–	Average of available gas exchange measurements
Z_R	0.3	0.3	m	Depth containing >80% of root mass (Fay et al., 2009)
α_1	0.25	0.25	MPa^{-1}	Vico and Porporato (2008)
α_2	3	3	–	Vico and Porporato (2008)
γ	227	365	μmol m^{-2} s^{-1}	Calibrated (Fig. 2)
λ^*	981	1913	μmol mol^{-1}	Manzoni et al. (2010)
η	1	25	–	von Caemmerer (2000)
ν	4	4	–	Daly et al. (2004)
Γ (25 °C)	36.9	0	μmol mol^{-1}	Leuning (1995)

temperature of 36.9 °C and obtained the base respiration and temperature sensitivity from linear regression of the log-transformed data ($\alpha = -2.1$ and $\beta = 0.24$, using Kirschbaum's notation). Since we assume vegetation characteristics are constant along the LYCOG, for consistency we also neglect atmospheric CO_2 effects on soil respiration.

3. Results and discussion

Model behavior was examined at three spatial scales. We first evaluated the performance of the atmospheric sub-model against observed velocity profiles (Section 3.1.1). We then modeled mean scalar concentrations and sources, as well as turbulent fluxes at the compartment level (Section 3.1.2). Finally, the entire chamber system was considered, and the responses of the CO_2 concentration gradient to changes in flow rate, species composition, and external environmental conditions were assessed (Section 3.1.3). The specific results refer to the LYCOG case study, but they qualitatively illustrate more general patterns that may be found in other closed systems.

3.1. Vertical profiles of mean longitudinal velocity

The vertical profiles of mean longitudinal velocity affect the advective component of the mass and energy balance equation (Eq. (2)) and the strength of the turbulent mixing (Eq. (4)). We assessed the performance of the implemented first-order closure scheme (Eqs. (3)–(5)) by comparing the computed $U(z)$ with measured vertical profiles at different positions along the chamber and at different flow rates (Fig. 3). Because our goal here is to test the transport model under a variety of conditions, we consider canopies differing in both LAI profile and species composition, while in the following sections we will focus on a single LAI profile and specify the vegetation type. The model captures the main features of the observed mean velocity profiles without adjustments in the parameters, confirming the generally good performance of this simple first-order closure scheme (here with a specified constant mixing length) in modeling the profiles of longitudinal velocity and vertical turbulent fluxes in dense canopies (Katul et al., 2004; Poggi et al., 2009, 2004).

Most models for greenhouse simulation assume the greenhouse as a vertically well-mixed environment imposed on the vegetation, and focus on the bulk energy balance, while neglecting vertical gradients of air velocity and turbulent transport (Boulard and Baille, 1993; Kindelan, 1980; Kittas et al., 2003; Roy et al., 2002; Singh et al., 2006; Soribe and Curry, 1973; Teitel et al., 2010). This simplification may lead to errors in the characterization of the canopy micro-environment (to which leaf gas exchange is sensitive) where vertical gradients are important (Fig. 3; see also Zhao et al., 2001). Moreover, this assumption has been examined for 'open systems'

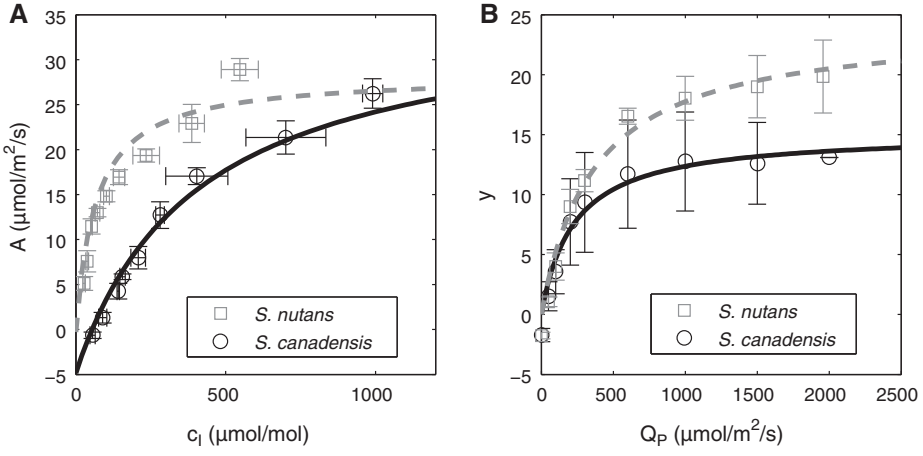

Fig. 2. Calibration of the leaf-level photosynthesis model (Eq. (10)). (A) CO_2 response and (B) light response curves for *S. canadensis* and *S. nutans* (on the *y*-axis in panel B, $y = (A + R_d)(\eta c_I + a_2) / \left[f_{a_1}(T_L)(\eta c_I - \Gamma)\right]$). In panel A, the curvature in the linearized photosynthesis model of Eq. (10) arises because C_A is the only source of variability for c_I, resulting in simultaneous increase of both c_I and $R_C C_A$.

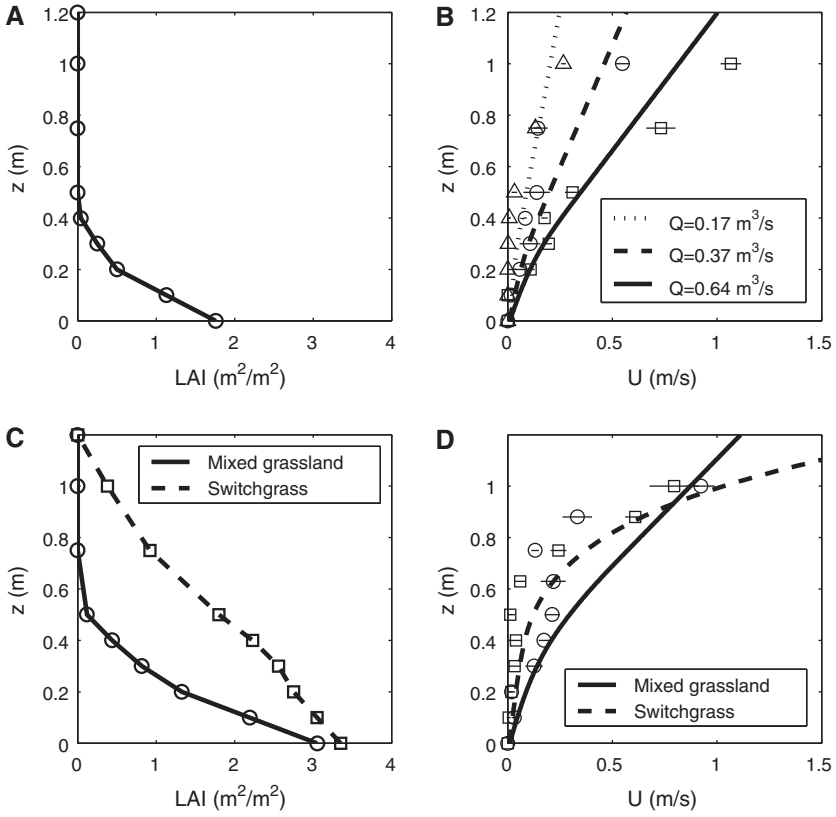

Fig. 3. (A and C) measured leaf area index profiles in three LYCOG plots. (B and D) measured (symbols) and modeled (lines) profiles of mean longitudinal velocity corresponding to the LAI profiles on the left (B, effect of air flow rate, Q, for given LAI profile; D, effect of different LAI profiles at a given flow rate).

by Juang et al. (2008) for a pine forest and was shown to be most significant for sensible heat fluxes and surface temperature predictions, which play a key role in the leaf energy balance and leaf temperature. To overcome this problem, some recent models employ direct numerical solution of the Navier–Stokes equations describing the greenhouse fluid dynamics (Boulard et al., 2002; Majdoubi et al., 2009). Compared to this computationally demanding method, two-dimensional approaches based on time-averaged equations (as employed here) are more efficient and provide reasonably good estimates of profiles of mean vertical velocity (Fig. 3). These time-averaged approaches can be readily integrated over seasonal, annual, and even inter-annual time scales thereby ensuring that all the key two-way interactions between the canopy and its micro-climate are accounted for across the widest possible ranges of environmental conditions (Siqueira et al., 2006). In essence, time-averaged approaches do not resolve all the scales characterizing turbulent eddies, but they account for the effects of turbulence on the micro-climate.

3.2. Results at the compartment level

Fig. 4 shows the mean scalar concentration, sources, and turbulent vertical fluxes in an individual 5-m long and 1.2-m tall compartment. Atmospheric CO_2 concentration is primarily depleted by the high photosynthetic activity in the central region of the canopy, where both leaf area density and light availability are high. Regions of high photosynthetic activity are also sources of water vapor, which accumulates longitudinally throughout the chamber. The depletion of c_A creates a local vertical concentration gradient that brings CO_2 from the soil surface and the upper regions towards the central, more photosynthetically active portion of the canopy. The downward vertical transport is more efficient than the transport from the soil surface because of higher mean velocity gradients (and consequently higher turbulent diffusion) in the upper part of the canopy (Fig. 3), which then drives higher turbulent fluxes (Eq. (4)). Water vapor fluxes move in the opposite direction (i.e., predominantly upward) because of the accumulation of water vapor in the central part of the canopy (also predicted in a greenhouse environment by Majdoubi et al. (2009)). Air temperature (lower left panel in Fig. 4) is highest near the ground level, but is similar to that of external air in the upper canopy region, where wind speed is sufficiently large and ensures adequate mixing. The vertical sensible heat flux is also highest at the bottom of the canopy because the ground surface heating propagates upward. Relatively high sensible heat transport also occurs around the top of the canopy where most of the solar radiation load occurs (but little evaporative cooling occurs because of low leaf area density and stomatal closure due to relatively large D), resulting in heating of the leaves. These temperature profiles are qualitatively similar to profiles obtained from direct numerical simulations for a greenhouse (Majdoubi et al., 2009), while taller vegetation in open systems tends to show the opposite pattern, with higher temperature around the top of the canopy at midday (Juang et al., 2008). Also in greenhouses, as the ventilation increases and with relatively uniform canopies, the negative air temperature gradient we predict may shift to a positive gradient due to stronger solar radiation interception at the top and effective mixing and cooling in the lower canopy (Zhao et al., 2001).

Sources and sinks of CO_2 and water vapor within the canopy (S_C and S_W, see right panels in Fig. 4) are primarily controlled by Fickian diffusion (Eqs. (8) and (9)), leaf physiological processes (Eq. (10)), light availability, and leaf area density. Local scalar concentrations change less along the vertical direction than light availability and leaf area, which are independent of position x in this homogeneous canopy. As a consequence, S_C and S_W are nearly homogeneous in the longitudinal direction, but vary significantly in the vertical direc-

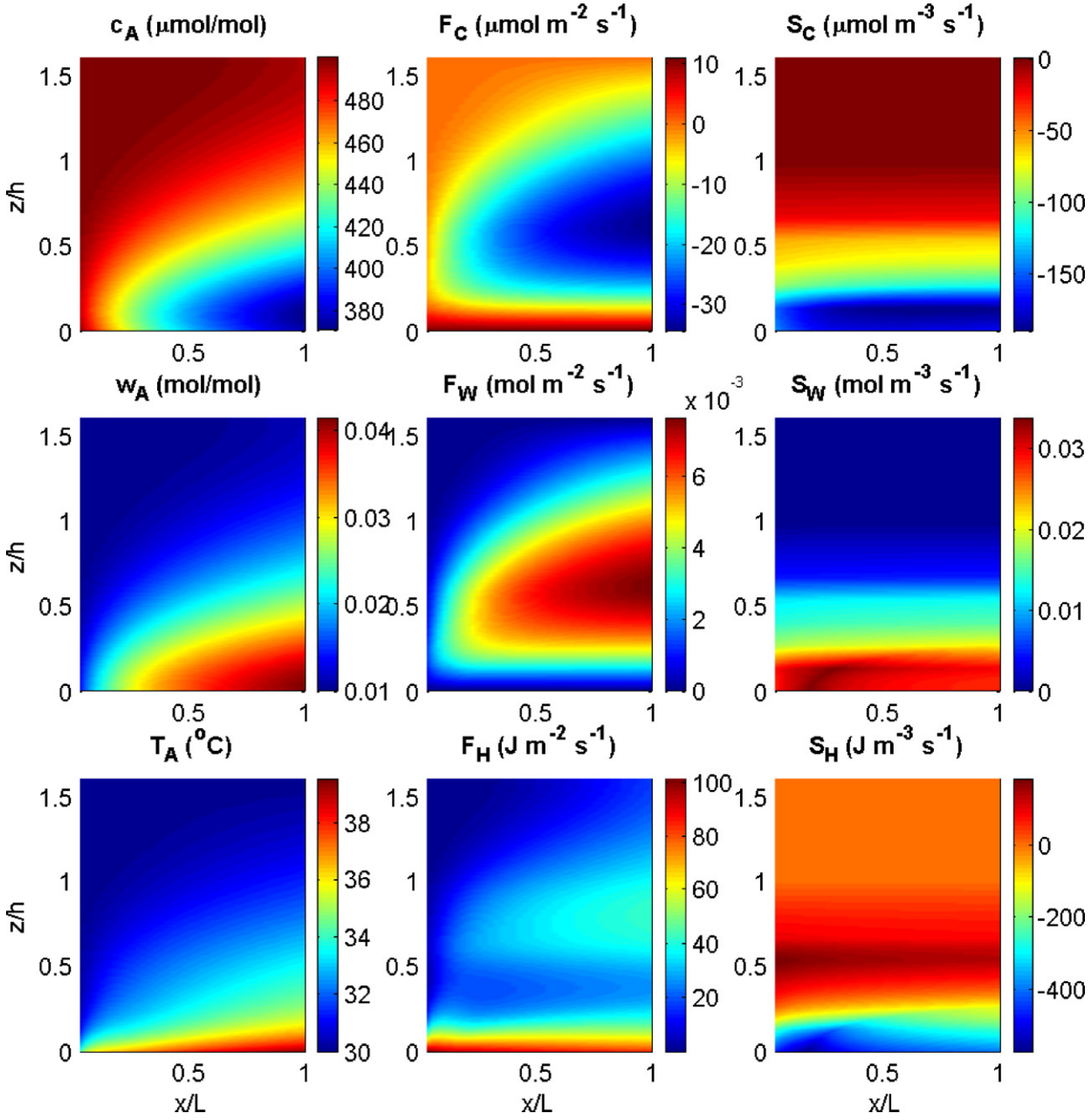

Fig. 4. Scalar concentration fields (left panels), vertical turbulent fluxes (central panels), and scalar sources and sinks (right panels), along a single compartment of length $L = 5$ m and height of 1.2 m ($h = 0.75$ m). Simulations refer to *Sorghastrum nutans*, with typical midday summer conditions at the LYCOG facility: $T_{A,IN} = 30\,^{\circ}$C, $c_{A,IN} = 500$ μmol mol^{-1}, $w_{A,IN} = 0.01$ mol mol^{-1}, total radiation 900 W m^{-2}, $w_s = 0.4$ m^3 m^{-3}, flow rate 0.2 m^3 s^{-1}.

tion. Because transpiration (and hence latent heat production) and solar radiation input do not vary appreciably along x, also the sensible heat source mainly varies vertically by virtue of the leaf energy balance. Sensible heat sources are particularly high in the bottom canopy layer, where part of leaf area is not actively transpiring and turbulent mixing is relatively weak. In contrast, the lower part of the canopy absorbs sensible heat ($S_H < 0$) converting it into latent heat through high transpiration.

The accumulation of sensible heat in the chambers due to relatively slow heat losses by conduction at the soil surface and interface between the polyethylene cover and ambient air leads to increased air and leaf temperature in the longitudinal direction. Fig. 5 illustrates how input air temperature and flow rate affect such an increase. At low flow rates, advection is poor and air temperature increases faster than at high flow rates. In these conditions the vapor pressure deficit also increases in the longitudinal direction, causing stomatal closure and inhibiting the evaporative cooling provided by transpiration. As a consequence, T_A increases sharply as the canopy converts virtually all the solar radiation input into sensible heat. The model captures the average temperature increase observed at the end of each of the LYCOG compartments of about 5 °C (with average daytime $T_{A,IN}$ between 23 and 30 °C and flow rate between 0.1 and 0.3 m^3 s^{-1}, see Fay et al. (2009)). Future experiments could be designed using model outputs as in Fig. 5 to optimize flow rate and chamber length so as to obtain a desired temperature gradient throughout the chambers, resulting in a compound elevated-temperature/enriched-CO_2 experiment.

Longitudinal accumulation of sensible heat is common in greenhouse systems as well (Kittas et al., 2003; Willits, 2003). Predictions from mathematical models that account for these longitudinal gradients are in agreement with our results of steeper gradients under

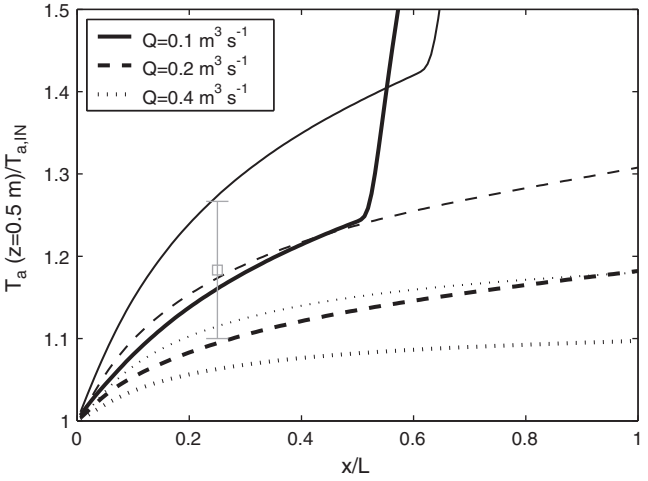

Fig. 5. Increase in air temperature at 0.5 m height along a single compartment (L = 20 m), for different input air temperatures $T_{A,IN}$ (thick lines, $T_{A,IN}$ = 30 °C, thin lines, $T_{A,IN}$ = 25 °C) and flow rates Q. The mean (and range) temperature increase at the LYCOG (where L = 5 m) is also shown (indicated by □; data from Fay et al., 2009). The simulations are for *S. nutans* under the same environmental conditions as in Fig. 4, except for varying $T_{A,IN}$ and Q.

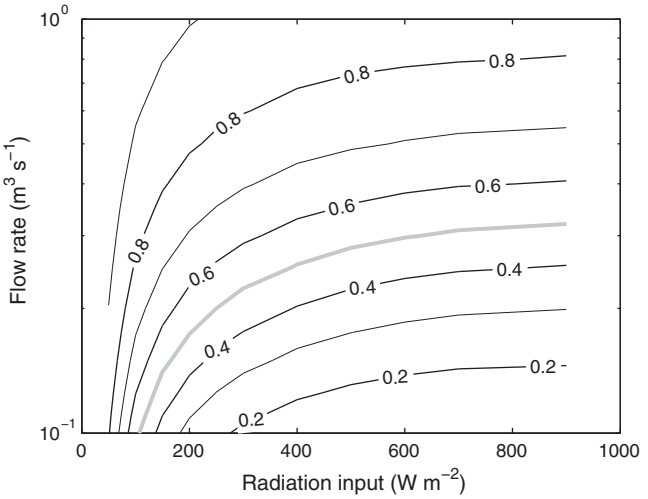

Fig. 7. Contour plot of the ratio of CO_2 concentration at the exit to that at the entrance of the chamber, for different combinations of flow rates (in logarithmic scale) and solar radiation levels. The thick gray line indicates the target for the LYCOG facility (a CO_2 concentration gradient from 500 to 250 μmol mol^{-1}, or $C_{A,OUT}/C_{A,IN}$ = 0.5, see Fay et al., 2009). The simulations are for *S. nutans* under the same environmental conditions as in Fig. 4, except for radiation input and air flow rate.

lower ventilation and higher air humidity (Kittas et al., 2003; Teitel et al., 2010; Willits, 2003).

3.3. Results at the whole chamber level

In general, a longer transit time of air in the chamber system allows a more efficient capture of CO_2 by plants, resulting in a steeper atmospheric CO_2 concentration gradient. This pattern is shown in Fig. 6 for idealized uniform canopies composed of either of the two dominant species grown in the LYCOG facility. The higher photosynthetic capacity of C4 *S. nutans* (Fig. 2) produces a stronger gradient than the C3 *S. canadensis* for any given flow rate. For the range of CO_2 concentration maintained at the LYCOG site (500–250 μmol mol^{-1}), the gradient of C_A is nearly constant because the curvature of the leaf-level CO_2 response is less important than the mixing processes at the canopy level. Additionally,

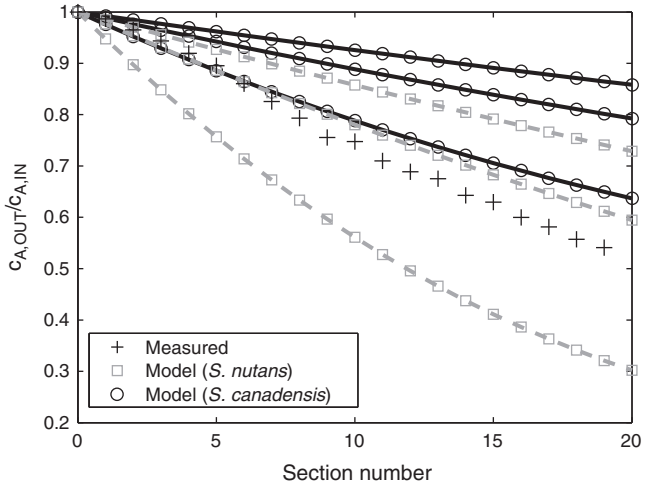

Fig. 6. Sensitivity of the air CO_2 concentration (expressed as ratio between CO_2 concentration at the exit and at the entrance of the chamber, $C_{A,OUT}/C_{A,IN}$) to changes in flow rate and species composition, along a sequence of 20, 5-m long compartments (as at the LYCOG facility). For each species, an increase in air flow rate flattens the curve (specific values of flow rate are 0.2, 0.4, and 0.6 m^3 s^{-1}; other external conditions as in Fig. 4). Measured mean $C_{A,OUT}/C_{A,IN}$ at the LYCOG facility are also shown for a visual comparison with model results.

soil respiration provides a large source of CO_2 close to the bulk leaf area that partly decouples photosynthesis from bulk atmospheric conditions. This weakens the leaf-level nonlinear effect of C_A on photosynthesis and contributes to the nearly linear longitudinal profile of C_A. The change in C_A per unit of change in distance along chambers decreases when C_A < 200 μmol mol^{-1} (see the simulation for *S. nutans* at low air flow rate) because photosynthetic capacity decreases sharply at low C_A (Fig. 2). Under typical summer conditions, the modeled C_A profiles for *S. nutans* slightly overestimate the slope of the average measured profile, while profiles for *S. canadensis* are flatter. Because about 75% of plant biomass is encompassed by C4 species at the LYCOG (mainly *S. nutans*, see Fay et al. (2009)), accounting for species heterogeneity in the model (even with an idealized homogeneous LAI profile) would easily improve the simulated C_A profile.

Fig. 7 illustrates the combined effect of solar radiation and air flow rate on the efficiency of the chamber system, expressed as the ratio between atmospheric CO_2 concentration at the exit to that at the entrance of the chamber, $C_{A,OUT}/C_{A,IN}$. Low flow rates (as in Fig. 6) and higher available light generally allow a stronger depletion of C_A because of increased transit time and photosynthetic activity, respectively, as observed in greenhouses as well (Teitel et al., 2010). However, at low flow rates and high external air temperature, reduced photosynthesis and sustained soil respiration result in a net accumulation of CO_2 (i.e., $C_{A,OUT}/C_{A,IN}$ > 1). Fig. 8 illustrates this effect, showing a transition occurring above $T_{A,IN}$ = 36 °C (a not uncommon value at the LYCOG site) as fan speed is reduced. At high flow rate the vegetation effectively cools the chamber air through transpiration, while evaporative cooling is impaired at lower flow rates, resulting in stomatal closure and decreased activity in the vegetation, which now only exchanges sensible heat with the atmosphere (Fig. 5 illustrates where this transition occurs in the longitudinal direction). The occurrence of this transition makes it difficult to maintain a prescribed $C_{A,OUT}/C_{A,IN}$ under some environmental conditions. The flow rate can be increased to avoid the break down of the C_A gradient (e.g., following upwards the solid black line in Fig. 8), but in this way the resulting $C_{A,OUT}/C_{A,IN}$ could differ from the prescribed value. The transition from vegetation that transpires rapidly and thereby provides effective evaporative cooling to vegetation that transpires little is sensitive to changes in air flow rate

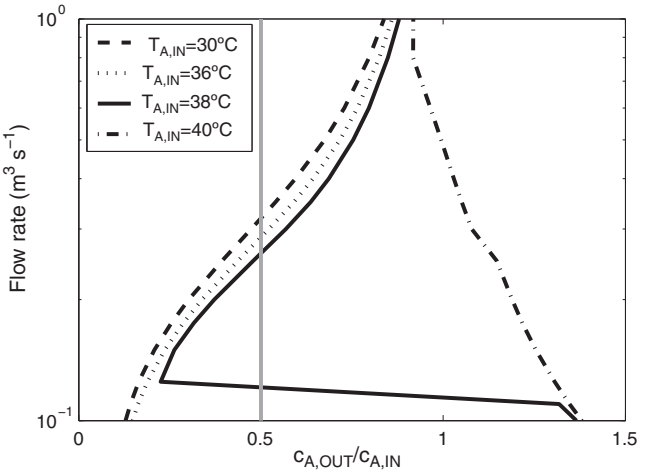

Fig. 8. Relationship between air flow rate (in logarithmic scale) and $C_{A,OUT}/C_{A,IN}$ at saturating light and different external air temperatures, $T_{A,IN}$. The thick gray line indicates the target $C_{A,OUT}/C_{A,IN}$ = 0.5 for the LYCOG facility. The simulations are for *S. nutans* under the same environmental conditions as in Fig. 4, except for the different $T_{A,IN}$ and air flow rate.

because air temperature, vapor pressure deficit, and plant physiological dynamics are strongly coupled to air flow, as showed in the previous analyses.

From an experimental operation perspective, Figs. 6 and 7 illustrate the air flow rates necessary to maintain a desired $C_{A,OUT}/C_{A,IN}$ for different radiation and temperature regimes. The target $C_{A,OUT}/C_{A,IN}$ = 0.5 for the LYCOG facility (highlighted by a thick gray line in Figs. 7 and 8) can be obtained by increasing the flow rate while radiation levels increase during the day. This is currently achieved through an empirical feedback control system that increases the flow rate when $C_{A,OUT}/C_{A,IN}$ < 0.5 is measured at the exit of the chamber (Fay et al., 2009). Note that typical flow rates in the LYCOG are lower than indicated in Fig. 7 because the actual canopy contains a variety of species that are not as efficient as *S. nutans* in taking up CO_2. Thus, when framing this problem as a model-assisted design approach for the LYCOG facility, species heterogeneity and their concomitant physiological, radiative, drag, and leaf area attributes would need to be fully accounted for.

This type of model-assisted design is commonly employed for greenhouses, where it is critical, as in the LYCOG, to maintain physiologically optimum temperature and humidity. Models have thus been used to implement efficient ventilation and evaporative cooling systems (Boulard and Baille, 1993; Kittas et al., 2003; Teitel et al., 2010; Willits, 2003), or to optimize air movement by modifying crop orientation (Majdoubi et al., 2009). Despite widespread application in greenhouse design, we are not aware of similar applications to ecosystem-level ecological experiments. Importantly, in applications to ecological experiments, the coupled biochemical and transport processes need to be accounted for. The few models that describe atmospheric CO_2 concentration, water vapor, and air temperature in a closed environment neglect several feedbacks between the leaf and its micro-environment and greatly simplify the leaf biochemistry (Teitel et al., 2010; Yang et al., 1990). While these simplified approaches are justified in the context of greenhouse design, they might lack the resolution necessary to address eco-physiological questions related to ecosystem response to climatic changes.

4. Conclusions

A vegetation–atmosphere gas exchange model is proposed to describe chamber systems used to investigate the effects of altered climatic conditions on ecosystem productivity. The model couples a description of leaf-scale physiology based on a water use optimality hypothesis to a simplified description of the atmospheric microclimate and boundary conditions characteristic of these closed systems. We parameterized the model to compute the main features of LYCOG experiment and tested it to assess the effects of plant species composition and environmental conditions on the simulated CO_2 concentration gradient. While some of the model assumptions and simplifications adopted here could be relaxed or improved, the model successfully reproduced key features of the LYCOG, namely (i) the sensitivity of the CO_2 concentration gradient to air flow rate (Fig. 6), (ii) the air temperature increase along a chamber and its dependence on flow rate and outside temperature (Fig. 5), (iii) the strong relationships among solar radiation, fan speed, and CO_2 concentration in the air outflow (Fig. 7), and (iv) the air temperature threshold above which the gradient can not be maintained because of loss of evaporative cooling and consequent accumulation of excessive sensible heat in the chamber (Fig. 8). Because the model allows mechanistic predictions of the effects of changes in air flow rate and external climatic conditions on ecosystem responses and the resulting CO_2 concentration gradient, it can be used as a tool to optimize chamber design (Figs. 7 and 8). Similarly, the sensitivity of model results to species composition (Fig. 6) permits investigation on how plant communities (see Fay et al., 2009) might impact the CO_2 gradient and to identify management options (e.g., changes in flow rate) for accommodating feedbacks from species change on environmental condition in the chamber.

The model also provides for the development of novel experimental designs to assess how climatic shifts impact ecological processes such as transpiration and photosynthesis. We showed that the length of a compartment and flow rate define a longitudinal air temperature gradient that can be used in compound elevated-temperature/enriched-CO_2 experiments. Additionally, simulations can be performed to assess the responses of this grassland ecosystem to a wide range of rainfall patterns that can not be reproduced in the original experiment. To achieve this goal, a full coupling of canopy gas exchange (described here) to a plant growth and soil moisture and nutrient cycling sub-model (e.g., Manzoni and Porporato, 2009; Porporato et al., 2003) that resolves daily-to-yearly time scales is necessary. Such detailed representation of soil–vegetation–atmosphere interactions represents a viable option to guide the design and management of these chamber systems, and can be used to formulate ecological hypothesis to be later tested in the field.

Acknowledgements

This research was partially supported by the U.S. Department of Agriculture (USDA grant 58-6206-7-029), by the United States Department of Energy (DOE) through the Office of Biological and Environmental Research (BER) Terrestrial Carbon Processes (TCP) program (FACE and NICCR grants: DE-FG02-95ER62083, DE-FC02-06ER64156), and by the National Science Foundation (NSF-EAR 0628342, NSF-EAR 0635787). We also thank Mario Siqueira for help with the implementation of CANVEG and two anonymous reviewers for their constructive comments.

Appendix A. List of symbols

Tables A1–A4 list all symbols used for atmosphere, canopy, leaf-level, and soil-to-leaf conductance calculations, respectively. Specific values for the physiological parameters of the species considered are reported in Table 1.

Table A1
Symbols used in the atmospheric fluid mechanic sub-model. Subscripts M and J respectively identify momentum and the different scalars (CO_2, $J = C$ [μmol mol^{-1}]; water vapor, $J = W$ [mol mol^{-1}]; sensible heat, $J = H$ [J mol^{-1}]); subscripts IN and OUT indicate chamber input and output.

Symbol	Explanation	Units
C_A, $C_{A,IN}$, $C_{A,OUT}$	CO_2 concentration	μmol mol^{-1}
D	Height of the drag force center of mass	m
H	Height of canopy top	m
k_t	Turbulent diffusivity	m^2 s^{-1}
w_A, $w_{A,IN}$, $w_{A,OUT}$	Water vapor concentration	mol mol^{-1}
$w_{sat}(T)$	Water vapor concentration at saturation	mol mol^{-1}
x	Longitudinal direction	m
z	Vertical direction	m
ℓ	Mixing length (Eq. (5))	m
L	Length of a compartment (LYCOG: 5 m)	m
C_d	Drag coefficient, $C_d = 0.3$	–
F_J, F_M	Vertical flux of scalar J or momentum	[J] mol m^{-2} s^{-1}, m^2 s^{-2}
L_{AD}	Leaf area density	m^2 m^{-3}
S_J	Source term for a generic scalar J	[J] s^{-1}
U	Mean longitudinal air velocity	m s^{-1}
T_A, $T_{A,IN}$, $T_{A,OUT}$	Air temperature	$^\circ$C
κ	Von Karman constant, $\kappa = 0.4$	–

Table A2
Symbols used in the radiation transfer and energy balance equations. Subscript i identifies the different wavebands (near infrared, $i = NIR$; visible, $i = V$).

Symbol	Explanation	Units
C_p	Air heat capacity, $C_p = 29.3$	J mol^{-1} $^\circ$C^{-1}
f_i	Solar radiation partitioning coefficients ($f_V = 0.45$, $f_{NIR} = 0.55$)	–
k	Extinction coefficient for black leaves ($k = 0.5/\cos\Psi$)	m^2 m^{-2}
k_D	Extinction coefficient for diffuse light ($k_D = 0.8$)	m^2 m^{-2}
H_G	Sensible heat flux between the ground surface and the atmosphere	W m^{-2}
Q	Air flow rate	m^3 s^{-1}
Q_n	Net absorbed radiation	W m^{-2}
Q_i	Direct or diffuse absorbed radiation in waveband i	W m^{-2}
$Q_i^\downarrow$	Radiation in waveband i at the top of the canopy	W m^{-2}
Q_P	Absorbed photosynthetic active radiation, $Q_P = 4.6Q_V$	μmol m^{-2} s^{-1}
Λ	Latent heat of vaporization (calculated after Bonan, 2008)	J mol^{-1}
ρ_i	Reflection coefficient in waveband i (Eq. (7))	–
σ	Stephan Boltzman constant, $\sigma = 5.67 \times 10^{-8}$	W m^{-2} K^{-4}
σ_i	Scattering coefficient in waveband i ($\sigma_V = 0.2$, $\sigma_{NIR} = 0.8$)	–
Ψ	Zenith angle	rad
ξ	Cumulative leaf area index profile, $\xi = \int_z^h LAI(z)\,dz$	m^2 m^{-2}

Table A3
Symbols used in the leaf gas exchange and energy balance equations. Subscript J identifies the different scalars (CO_2, $J = C$ [μmol mol^{-1}]; water vapor, $J = W$ [mol mol^{-1}]; sensible heat, $J = H$ [J mol^{-1}]).

Symbol	Explanation	Units
a_1, $a_{1,WW}$	Photosynthetic rate (WW, well-watered conditions)	μmol m^{-2} s^{-1}
a_2	Half saturation constant in Eq. (10)	μmol mol^{-1}
c_I	Internal CO_2 concentration	μmol mol^{-1}
d_L	Average leaf width	m
f	Gain function, $f = A - \lambda E$	μmol m^{-2} s^{-1}
$g_{B,J}$	Leaf boundary layer conductance for scalar J	mol m^{-2} s^{-1}
$g_{IA,J}$	Leaf-bulk atmosphere conductance for scalar J	mol m^{-2} s^{-1}
$g_{S,C,max}$	Maximum stomatal conductance to CO_2	mol m^{-2} s^{-1}
$g_{S,J}$	Stomatal conductance to scalar J	mol m^{-2} s^{-1}
$g^*_{S,C}$	Initial guess for stomatal conductance to CO_2	mol m^{-2} s^{-1}
$\chi_{B,W:C}$	Ratio between leaf boundary layer conductances to water vapor and CO_2, $\chi_{B,W:C} = g_{B,W}/g_{B,C} = 1.34$	–
$\chi_{S,W:C}$	Ratio between stomatal conductances to water vapor and CO_2, $\chi_{S,W:C} = g_{S,W}/g_{S,C} = 1.65$	–
$\chi_{B,H:C}$	Ratio between leaf boundary layer conductances to sensible heat and CO_2, $\chi_{B,H:C} = g_{B,H}/g_{B,C} = 1.23$	–
s	$dw_{sat}(T)/dT$	mol mol^{-1} $^\circ$C^{-1}
A	Leaf net CO_2 assimilation	μmol m^{-2} s^{-1}
D	Atmospheric vapor pressure deficit, $D = w_{sat}(T_A) - w_A$	mol mol^{-1}
E	Leaf transpiration	mol m^{-2} s^{-1}
K_C	Michaelis constant for carboxylation	μmol mol^{-1}
K_O	Michaelis constant for oxygenation	mol mol^{-1}
$[O_2]$	Oxygen concentration, $[O_2] = 0.21$	mol mol^{-1}
R_C	Long-term average C_I/C_A (Eq. (10))	–
R_d	Mitochondrial respiration	μmol m^{-2} s^{-1}
α_1, α_2	Parameters for $a_1(\Psi_L)$ in Eq. (11)	Different units
γ	Half-saturation constant of the light response (Eq. (10))	μmol m^{-2} s^{-1}
λ	Marginal water use efficiency, $\lambda = \partial A/\partial E$	μmol mol^{-1}
λ^*	Marginal water use efficiency at $C_A = 400$ μmol mol^{-1}	μmol mol^{-1}
Γ	CO_2 compensation point	μmol mol^{-1}
Ψ_L	Leaf water potential	MPa

Table A4
Symbols used in the soil-to-leaf conductance model.

Symbol	Explanation	Units
d_R	Average root radius	m
g_{SR}, g_{RL}	Soil-to-root (Eq. (17)) and root-to-leaf conductances	mol m^{-2} s^{-1} MPa^{-1}
g_{SL}	Soil-to-leaf conductance, $g_{SL} = g_{SR}g_{RL}/(g_{SR} + g_{RL})$	mol m^{-2} s^{-1} MPa^{-1}
$K_H(\Psi_s)$	Soil hydraulic conductivity	m s^{-1}
R_{AI}	Root area index	m^2 m^{-2}
w_S	Relative volumetric soil moisture	m^3 m^{-3}
Z_R	Rooting depth	m
φ	Unit conversion factor ($\varphi = 10^9/18 \times 9.81$)	mol m^{-2} MPa^{-1}
ν	Exponent of the correction factor for root elongation	–
Ψ_S	Soil water potential	MPa

Appendix B. Conditions for the application of first-order closure principles

For completeness, the necessary conditions for the application of first-order closure principles and our rationale for choosing them for this particular application are presented here. We refer to Juang et al. (2008) and references therein for more detailed descriptions of the budget equation and closure models employed in this derivation. For a stationary and planar homogeneous high Reynolds number and Peclet number flows, the budget equation for an arbitrary scalar (J) flux is given by

$$\frac{\partial \left\langle \overline{w'J'} \right\rangle}{\partial t} = 0 = \underbrace{-\left\langle \overline{w'w'} \right\rangle \frac{\partial \left\langle \bar{J} \right\rangle}{\partial z}}_{I} \underbrace{-\frac{\partial \left\langle \overline{w'w'J'} \right\rangle}{\partial z}}_{II} \underbrace{-\frac{1}{\rho}\left\langle J' \overline{\frac{\partial p'}{\partial z}} \right\rangle}_{III} + \underbrace{\frac{g}{\left\langle \overline{T_A} \right\rangle} \left\langle \overline{T'_A J'} \right\rangle}_{IV}, \tag{B1}$$

where w', T'_A, p', J' represent fluctuations in vertical velocity, air temperature, air pressure, and scalar concentration, ρ is the air density, g the gravitational acceleration, and overbar and angle brackets indicate time and planar-averaging, respectively. The terms on the right hand side of Eq. (B1) are defined as follows: the first term (I) is the flux production, the second term (II) is the turbulent flux transport, the third term (III) is the scalar–pressure interaction (a de-correlation or dissipation term), and the fourth term (IV) is the buoyancy production (or dissipation).

If the dissipation term is parameterized as:

$$\frac{1}{\rho}\left\langle J' \overline{\frac{\partial p'}{\partial z}} \right\rangle = \frac{C_4}{\tau} \left\langle \overline{w'J'} \right\rangle, \tag{B2}$$

and the flux transport term is given as

$$\left\langle \overline{w'w'J'} \right\rangle = -C_5 \tau \left\langle \overline{w'w'} \right\rangle \frac{\partial \left\langle \overline{w'J'} \right\rangle}{\partial z} = -C_5 \tau \sigma_w^2 S_J, \tag{B3}$$

then combining Eqs. (B1)–(B3) yields

$$\left\langle \overline{w'J'} \right\rangle = \frac{\tau}{C_4}\left[-\sigma_w^2 \frac{\partial \left\langle \bar{J} \right\rangle}{\partial z} + C_5 \frac{\partial \left(\tau \sigma_w^2 S_J \right)}{\partial z} + \frac{g}{\left\langle \overline{T_A} \right\rangle} \left\langle \overline{T'_A J'} \right\rangle \right], \tag{B4}$$

where τ is a relaxation time scale defined as the ratio of the turbulent kinetic energy to its dissipation rate, C_4 and C_5 are similarity constants, $\sigma_w^2 = \overline{w'w'}$, and S_J is, as before, the scalar source (or sink) term. Hence, we expect that when

$$\left| \sigma_w^2 \frac{\partial \left\langle \bar{J} \right\rangle}{\partial z} \right| >> \left| C_5 \frac{\partial \left(\tau \sigma_w^2 S_J \right)}{\partial z} + \frac{g}{\left\langle \overline{T_A} \right\rangle} \left\langle \overline{T'_A J'} \right\rangle \right|, \tag{B5}$$

first-order closure arguments inside the canopy hold.

For the LYCOG canopy, it is likely that σ_w^2 remains large inside the canopy. Moreover, given the ground heating and CO_2 emission, and the concentration of foliage near the ground (Fig. 3), much of the canopy leaf area is experiencing strong vertical gradients (at least for air temperature, water vapor, and CO_2). Moreover, much of the canopy height has small leaf area density (i.e., S_J is small except close to the ground) so that $\partial \left(\tau \sigma_w^2 S_\xi \right) / \partial z$ is expected to be small except in the lower layers of the canopy, where the lower-boundary conditions generate the largest gradients (especially for T_A). Hence, the LYCOG setup favors a situation in which the condition in (B5) is likely to hold, though we emphasize that condition (B5) is not generally satisfied for an arbitrary canopy.

References

Baldocchi, D., Meyers, T., 1998. On using eco-physiological, micrometeorological and biogeochemical theory to evaluate carbon dioxide, water vapor and trace gas fluxes over vegetation: a perspective. Agricultural and Forest Meteorology 90, 1–25.

Berninger, F., Hari, P., 1993. Optimal regulation of gas-exchange – evidence from field data. Annals of Botany 71, 135–140.

Bonan, G.B., 2008. Ecological Climatology. Concepts and Applications, 2nd ed. Cambridge University Press, New York, 550 pp.

Boulard, T., Baille, A., 1993. A simple greenhouse climate control model incorporating effects of ventilation and evaporative cooling. Agricultural and Forest Meteorology 65, 145–157.

Boulard, T., Kittas, C., Roy, J.C., Wang, S., 2002. Convective and ventilation transfers in greenhouses, part 2: determination of the distributed greenhouse climate. Biosystems Engineering 83, 129–147.

Buckley, T.N., 2008. The role of stomatal acclimation in modelling tree adaptation to high CO_2. Journal of Experimental Botany 59, 1951–1961.

Buckley, T.N., Miller, J.M., Farquhar, G.D., 2002. The mathematics of linked optimisation for water and nitrogen use in a canopy. Silva Fennica 36, 639–669.

Campbell, G.S., Norman, J.M., 1998. An Introduction to Environmental Biophysics, 2nd ed. Springer, 286 pp.

Cowan, I., Farquhar, G.D., 1977. Stomatal Function in Relation to Leaf Metabolism an Environment. Integration of Activity in the Higher Plants. Symposia of the Society of Experimental Biology. Cambridge University Press, pp. 471–505.

Daly, E., Porporato, A., Rodriguez-Iturbe, I., 2004. Coupled dynamics of photosynthesis, transpiration, and soil water balance. Part I: upscaling from hourly to daily level. Journal of Hydrometeorology 5, 546–558.

dePury, D.G.G., Farquhar, G.D., 1997. Simple scaling of photosynthesis from leaves to canopies without the errors of big-leaf models. Plant Cell and Environment 20, 537–557.

Farquhar, G.D., Caemmerer, S.V., Berry, J.A., 1980. A biochemical-model of photosynthetic CO_2 assimilation in leaves of C-3 species. Planta 149, 78–90.

Fay, P.A., Kelley, A.M., Procter, A.C., Hui, D., Jin, V.L., Jackson, R.B., Johnson, H.B., Polley, H.W., 2009. Primary productivity and water balance of grassland vegetation on three soils in a continuous CO_2 gradient: initial results from the Lysimeter CO_2 gradient experiment. Ecosystems 12, 699–714.

Friend, A.D., 1995. PGEN – an integrated model of leaf photosynthesis, transpiration, and conductance. Ecological Modelling 77, 233–255.

Goudriaan, J., van Laar, H.H., 1994. Modelling Potential Crop Growth Processes: Textbook with Exercises. Kluwer Academic Publisher, 239 pp.

Hari, P., Mäkelä, A., Korpilahti, E., Holmberg, M., 1986. Optimal control of gas exchange. Tree Physiology 2, 169–175.

Hsieh, C.I., Katul, G., 2009. The Lagrangian stochastic model for estimating footprint and water vapor fluxes over inhomogeneous surfaces. International Journal of Biometeorology 53, 87–100.

Jackson, R.B., Mooney, H.A., Schulze, E.D., 1997. A global budget for fine root biomass, surface area, and nutrient contents. Proceedings of the National Academy of Sciences of the United States of America 94, 7362–7366.

Johnson, H.B., Polley, H.W., Whitis, R.P., 2000. Elongated chambers for field studies across atmospheric CO_2 gradients. Functional Ecology 14, 388–396.

Juang, J.Y., Katul, G.G., Siqueira, M.B., Stoy, P.C., McCarthy, H.R., 2008. Investigating a hierarchy of Eulerian closure models for scalar transfer inside forested canopies. Boundary-Layer Meteorology 128, 1–32.

Katul, G., Manzoni, S., Palmroth, S., Oren, R., 2010. A stomatal optimization theory to describe the effects of atmospheric CO_2 on leaf photosynthesis and transpiration. Annals of Botany 105, 431–442.

Katul, G., Palmroth, S., Oren, R., 2009. Leaf stomatal responses to vapour pressure deficit under current and CO_2-enriched atmosphere explained by the economics of gas exchange. Plant Cell and Environment 32, 968–979.

Katul, G.G., Mahrt, L., Poggi, D., Sanz, C., 2004. One- and two-equation models for canopy turbulence. Boundary-Layer Meteorology 113, 81–109.

Kindelan, M., 1980. Dynamic modeling of greenhouse environment. Transactions of the ASAE 23, 1232–1239.

Kirschbaum, M.U.F., 1995. The temperature-dependence of soil organic-matter decomposition, and the effect of global warming on soil organic-C storage. Soil Biology & Biochemistry 27, 753–760.

Kittas, C., Bartzanas, T., Jaffrin, A., 2003. Temperature gradients in a partially shaded large greenhouse equipped with evaporative cooling pads. Biosystems Engineering 85, 87–94.

Lai, C.T., Katul, G., Butnor, J., Siqueira, M., Ellsworth, D., Maier, C., Johnsen, K., McKeand, S., Oren, R., 2002. Modelling the limits on the response of net carbon exchange to fertilization in a south-eastern pine forest. Plant Cell and Environment 25, 1095–1119.

Laio, F., Porporato, A., Fernandez-Illescas, C.P., Rodriguez-Iturbe, I., 2001. Plants in water-controlled ecosystems: active role in hydrologic processes and response to water stress – IV. Discussion of real cases. Advances in Water Resources 24, 745–762.

Landsberg, J.J., Waring, R.H., 1997. A generalised model of forest productivity using simplified concepts of radiation-use efficiency, carbon balance and partitioning. Forest Ecology and Management 95, 209–228.

Leuning, R., 1995. A critical-appraisal of a combined stomatal-photosynthesis model for C-3 plants. Plant Cell and Environment 18, 339–355.

Leuning, R., Kelliher, F.M., Depury, D.G.G., Schulze, E.D., 1995. Leaf nitrogen, photosynthesis, conductance and transpiration – scaling from leaves to canopies. Plant Cell and Environment 18, 1183–1200.

Majdoubi, H., Boulard, T., Fatnassi, H., Bouirden, L., 2009. Airflow and microclimate patterns in a one-hectare Canary type greenhouse: an experimental and CFD assisted study. Agricultural and Forest Meteorology 149, 1050–1062.

Manzoni, S., Porporato, A., 2009. Soil carbon and nitrogen mineralization: theory and models across scales. Soil Biology & Biochemistry 41, 1355–1379.

Manzoni, S., Vico, G., Katul, G., Fay, P.A., Polley, H.W., Palmroth, S., Porporato, A., 2010. Optimizing stomatal conductance for maximum carbon gain under water stress conditions. Functional Ecology (Under Revision).

Poggi, D., Krug, C., Katul, G.G., 2009. Hydraulic resistance of submerged rigid vegetation derived from first-order closure models. Water Resources Research, 45, W10442, doi:10.1029/2008WR007373.

Poggi, D., Porporato, A., Ridolfi, L., Albertson, J.D., Katul, G.G., 2004. The effect of vegetation density on canopy sub-layer turbulence. Boundary-Layer Meteorology 111, 565–587.

Polley, H.W., Johnson, H.B., Fay, P.A., Sanabria, J., 2008. Initial response of evapotranspiration from tallgrass prairie vegetation to CO_2 at subambient to elevated concentrations. Functional Ecology 22, 163–171.

Porporato, A., D'Odorico, P., Laio, F., Rodriguez-Iturbe, I., 2003. Hydrologic controls on soil carbon and nitrogen cycles. I. Modeling scheme. Advances in Water Resources 26, 45–58.

Rao, K.S., Wyngaard, J.C., Coté, O.R., 1974. Local advection of momentum, heat, and moisture in micrometeorology. Boundary-Layer Meteorology 7, 331–348.

Roy, J.C., Boulard, T., Kittas, C., Wang, S., 2002. Convective and ventilation transfers in greenhouses. Part 1: the greenhouse considered as a perfectly stirred tank. Biosystems Engineering 83, 1–20.

Running, S.W., Gower, S.T., 1991. Forest-BGC, a general-model of forest ecosystem processes for regional applications 2. Dynamic carbon allocation and nitrogen budgets. Tree Physiology 9, 147–160.

Singh, G., Singh, P.P., Lubana, P.P.S., Singh, K.G., 2006. Formulation and validation of a mathematical model of the microclimate of a greenhouse. Renewable Energy 31, 1541–1560.

Siqueira, M., Katul, G., Porporato, A., 2009. Soil moisture feedbacks on convection triggers: the role of soil–plant hydrodynamics. Journal of Hydrometeorology 10, 96–112.

Siqueira, M.B., Katul, G.G., Sampson, D.A., Stoy, P.C., Juang, J.Y., McCarthy, H.R., Oren, R., 2006. Multiscale model intercomparisons of CO_2 and H_2O exchange rates in a maturing southeastern US pine forest. Global Change Biology 12, 1189–1207.

Soribe, F.I., Curry, R.B., 1973. Simulation of lettuce growth in an air-supported plastic greenhouse. Journal of Agricultural Engineering Research 18, 133–140.

Spitters, C.J.T., 1986. Separating the diffuse and direct component of global radiation and its implications for modeling canopy photosynthesis. 2. Calculation of canopy photosynthesis. Agricultural and Forest Meteorology 38, 231–242.

Stoy, P.C., Richardson, A.D., Baldocchi, D.D., Katul, G.G., Stanovick, J., Mahecha, M.D., Reichstein, M., Detto, M., Law, B.E., Wohlfahrt, G., Arriga, N., Campos, J., McCaughey, J.H., Montagnani, L., Paw U, K.T., Sevanto, S., Williams, M., 2009. Biosphere-atmosphere exchange of CO_2 in relation to climate: a cross-biome analysis across multiple time scales. Biogeosciences 6, 2297–2312.

Teitel, M., Atias, M., Barak, M., 2010. Gradients of temperature, humidity and CO_2 along a fan-ventilated greenhouse. Biosystems Engineering 106, 166–174.

Thornley, J.H.M., Johnson, I.R., 1990. Plant and Crop Modelling: A Mathematical Approach to Plant and Crop Physiology. Clarendon Press, Oxford, 669 pp.

Tuzet, A., Perrier, A., Leuning, R., 2003. A coupled model of stomatal conductance, photosynthesis and transpiration. Plant Cell and Environment 26, 1097–1116.

Vico, G., Porporato, A., 2008. Modelling C3 and C4 photosynthesis under water-stressed conditions. Plant and Soil 313, 187–203.

von Caemmerer, S., 2000. Biochemical Models of Leaf Photosynthesis. CSIRO Publishing, 165 pp.

Williams, M., Rastetter, E.B., Fernandes, D.N., Goulden, M.L., Wofsy, S.C., Shaver, G.R., Melillo, J.M., Munger, J.W., Fan, S.M., Nadelhoffer, K.J., 1996. Modelling the soil–plant-atmosphere continuum in a *Quercus-Acer* stand at Harvard forest: the regulation of stomatal conductance by light, nitrogen and soil/plant hydraulic properties. Plant Cell and Environment 19, 911–927.

Willits, D.H., 2003. Cooling fan-ventilated greenhouses: a modelling study. Biosystems Engineering 84, 315–329.

Yang, X., Short, T.H., Fox, R.D., Bauerle, W.L., 1990. Dynamic modeling of the microclimate of a greenhouse cucumber row-crop. 1. Theoretical-model. Transactions of the ASAE 33, 1701–1709.

Zhao, Y., Teitel, M., Barak, M., 2001. Vertical temperature and humidity gradients in a naturally ventilated greenhouse. Journal of Agricultural Engineering Research 78, 431–436.